PCCP

PAPER

View Article Online
View Journal | View Issue

Cite this: *Phys. Chem. Chem. Phys.*, 2014, **16**, 11864

Effects of hydrogen bonding interactions on the redox potential and molecular vibrations of plastoquinone as studied using density functional theory calculations†

Ryota Ashizawa and Takumi Noguchi*

Received 8th November 2013,
Accepted 23rd December 2013

DOI: 10.1039/c3cp54742f

www.rsc.org/pccp

The effects of H-bonding on the redox potential and molecular vibrations of plastoquinone (PQ) that functions as a primary and a secondary quinone electron acceptor (Q_A and Q_B, respectively) in photosystem II (PSII) in plants and cyanobacteria were investigated using density functional theory calculations. Calculations were performed on the neutral and semiquinone anion forms of PQ and its H-bonded complexes, which form H-bonds with water molecules, or using amino acid models mimicking the interactions of Q_A and Q_B. The calculated redox potential (E^o) of PQ showed a linear relationship with the number of H-bonds, and the E^o increased by +100–200 mV with the addition of one H-bond. Vibrational analysis of the model PQ complexes showed that the CO stretching vibrations of neutral PQ are sensitive to the number and symmetry of H-bonding interactions, providing criteria to determine the H-bonding structure. Although no specific trend in the H-bonding dependency was found for anionic PQ, complex spectral features in the CO stretching region due to significant couplings with other PQ vibrations and the vibrations of H-bonding amino acids are useful monitors of the change in the H-bonding structure of anionic PQ in proteins. The calculated E^o values and infrared spectra of the Q_A and Q_B models are consistent with the view that one additional H-bond to Q_B from D1-Ser264 largely contributes to the redox potential gap between Q_A and Q_B in PSII.

Introduction

Photosystem II (PSII) is one of the major protein complexes that are involved in photosynthetic energy conversion occurring in plants and cyanobacteria. The most important function of PSII is abstracting electrons necessary for CO_2 reduction from water molecules using light energy. In PSII, primary charge separation takes place from the excited state of chlorophylls making a charged pair between the chlorophyll dimer (P680) and the pheophytin electron acceptor (Pheo), $P680^+Pheo^-$.[1,2] On the electron donor side, $P680^+$ abstracts an electron from the Mn_4Ca cluster, the catalytic site of water oxidation, *via* a redox-active tyrosine Y_Z.[3–6] After four turnover reactions, two water molecules are oxidized to one oxygen molecule and four protons generating four electrons. On the electron acceptor side, an electron is transferred from $Pheo^-$ to the primary quinone electron acceptor (Q_A), and then to the secondary quinone electron acceptor (Q_B).[7] When Q_B is doubly reduced by two electron transfer reactions, it is converted to a quinol molecule by binding two protons and is released from the Q_B site into thylakoid membranes.[7]

Both Q_A and Q_B consist of a plastoquinone-9 (PQ-9) molecule (Fig. 1B) bound to different sites in PSII. The mid-point redox potential (E_m) for one-electron reduction of Q_A has been

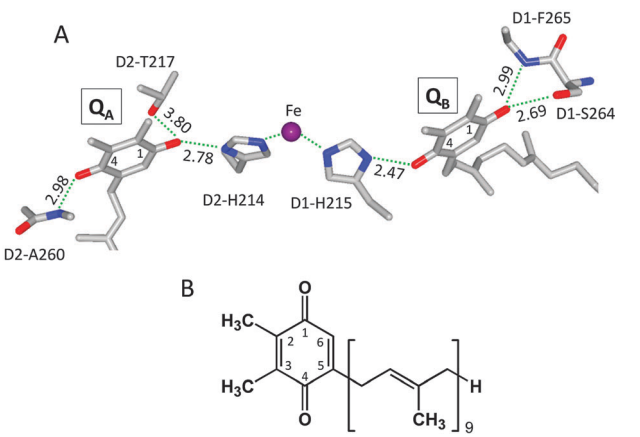

Fig. 1 (A) The structure of the Q_A and Q_B binding sites deduced from the X-ray crystal structure of PSII at 1.9 Å resolution (PDB code 3ARC).[22] (B) The chemical structure of plastoquione-9.

Division of Material Science, Graduate School of Science, Nagoya University, Furo-cho, Chikusa-ku, Nagoya, 464-8602, Japan.
E-mail: tnoguchi@bio.phys.nagoya-u.ac.jp

† Electronic supplementary information (ESI) available: Optimized geometries of semiquinone anions in plastoquinone complexes H-bonded to water molecules and amino acid models. See DOI: 10.1039/c3cp54742f

measured to be −80 mV in intact PSII membranes from spinach,[8] while E_m for one-electron reduction of Q_B has been estimated to be higher than that of Q_A by ∼+80 mV.[9,10] This E_m gap generates a driving force for smooth electron transfer from Q_A to Q_B. It is also known that E_m of Q_A increases by ∼140 mV upon depletion of the Mn_4Ca cluster[8,11] and shifts by ∼±50 mV by binding different types of herbicide at the Q_B site.[12] These E_m shifts change the kinetics of redox reactions and charge recombination pathways, resulting in inhibition or acceleration of photodamage in PSII.[12–15] The E_m gap between Q_A and Q_B as well as the E_m shifts of Q_A should arise from the changes in the protein environments at the Q_A and Q_B binding sites.[16–21] In particular, direct interactions of the C═O groups of PQ through H-bonds with proteins should be a significant factor to determine the E_m values of Q_A and Q_B.

The recent high-resolution (1.9 Å) X-ray structure of PSII complexes from the cyanobacterium *Thermosynechococcus vulcanus*[22] showed the structures of the Q_A and Q_B binding sites (Fig. 1A). They are located around the non-heme iron center with a pseudo C_2 symmetry, although the quinone rings are oriented in opposite ways, *i.e.*, the C(1)═O of Q_A and the C(4)═O of Q_B are directed to the central non-heme iron (Fig. 1A). The molecular interactions of Q_A and Q_B are very similar. The oxygen atoms of C(1)═O and C(4)═O of Q_A are at H-bond distances from the imidazole nitrogen of D2-H214 (2.78 Å) and the backbone nitrogen of D2-A260 (2.98 Å), respectively, while those of the C(4)═O and C(1)═O of Q_B are at H-bond distances from the imidazole nitrogen of D1-H215 (2.47 Å) and the backbone nitrogen of D1-F265 (2.99 Å), respectively. A significant difference, however, is that Q_B seems to have an additional H-bond at C(1)═O with the OH group of D1-S264 (2.69 Å). Although the OH of D2-T217 is also located near the C(1)═O of Q_A, the distance is a little too far (3.80 Å) to form a H-bond. Thus, from the X-ray structure of PSII,[22] Q_A seems to have two H-bonds, whereas Q_B seems to have three H-bonds. However, this X-ray structure without the information of hydrogen atoms cannot provide a definite conclusion about the H-bonding structures of Q_A and Q_B. For example, if the proton of the D1-S264 OH is directed to the imidazole of D1-H252 (the distance between the O (S264) and N (H252) atoms is 2.77 Å), there is no H-bond between D1-S264 and Q_B.[16] Also, D2-T217 can be H-bonded to the Q_A C(1)═O by changing the conformation of the side chain.[16] It is possible that the local structure in the PSII crystal at cryogenic temperature is rather different from the real structure in a physiological state at room temperature. Also, the H-bonding structures of Q_A and Q_B could change upon their reduction to semiquinone anions and some treatments such as Mn_4Ca depletion and herbicide binding.[16]

One of the powerful methods to study the H-bonding interactions of quinone molecules in photosynthetic proteins is light-induced Fourier transform infrared (FTIR) difference spectroscopy.[23–25] This spectroscopy can detect the changes in the structure and interactions of a quinone cofactor upon its photoreduction together with the structural changes in surrounding protein moieties as effects on the normal mode vibrations of the quinone and proteins. FTIR difference spectra of Q_A and Q_B (ubiquinone or menaquinone) in bacterial reaction centers,[26–30] and those (PQ-9) of PSII,[17,31,32] and A_1 (vitamin K_1) in PSI[33,34] have been obtained and analyzed by isotope substitution of quinone and the surrounding amino acid residues. In addition, electrochemically-induced FTIR difference measurements of quinones in organic solvents have been performed.[35,36] However, the effects of H-bonding interactions on the normal mode vibrations of neutral and anionic forms of quinones remain poorly understood.

Quantum chemical calculation is a particularly important tool to quantitatively investigate the effects of H-bonding interactions on the redox potentials and molecular vibrations of quinone molecules. In experimental systems of homogeneous solutions, it is difficult to realize asymmetric H-bonding structures with different H-bonding partners in the individual C═O groups, which are usually found in proteins. However, in calculations, such situations are readily realized by assuming model H-bonded complexes with intended H-bonding partners. A number of theoretical studies of quantum chemical calculations, especially using the density functional theory (DFT) method, have been performed to estimate redox potentials[37–41] and normal mode vibrations[17,42–48] for various quinone molecules. Some of the studies treat quinone models with H-bonds mostly with water molecules at the C═O groups to obtain the information on the effect of H-bonds.[17,44,46–48] However, systematic calculations using quinone models, especially those of PQ, with different H-bonding structures have not yet been investigated. Recent QM/MM calculations, in which protein environments around quinone molecules are involved in calculations, well reproduced vibrational and spin properties of quinones in bacterial reaction centers.[49–51] Although such a QM/MM approach is very important for reproduction of spectra and assignments of bands, involvement of all the effects of protein moieties, in contrast, makes it rather difficult to understand pure effects of H-bonding interactions on the energy and vibrations.

In this study, we have systematically investigated the effects of H-bonding interactions on the redox potential and normal mode vibrations of PQ using DFT calculations. For this purpose, we have performed calculations for the neutral and semiquinone anion forms of a PQ model and its H-bonded complexes, which have a different number of H-bonds with water molecules as simple H-bonding partners or with amino acid models mimicking the H-bonding interactions of Q_A and Q_B in PSII. The results of this work provided theoretical bases for interpretation of the Q_A^--minus-Q_A and Q_B^--minus-Q_B FTIR difference spectra to study the H-bonding structures in proteins and to understand the factors that determine the E_m of Q_A and Q_B in PSII.

Computational methods

Molecular orbital calculations were performed using the Gaussian09 program package.[52] The B3LYP functional[53,54] with the 6-31+G(d) basis set was used to optimize the geometries of the PQ models in both neutral and semiquinone anion forms.

Using the obtained optimized geometries, electronic energies were calculated at the B3LYP/6-311+G(3df,3pd) level in the gas phase and in solvents with different dielectric constants using IEF-PCM (PCM calculations using the integrated equation formalism model) approximation.[55–57] Six solvent parameters included in Gaussian09 were used: argon (ε = 1.4), benzene (ε = 2.2), chloroform (ε = 4.9), dichloroethane (ε = 10.4), acetone (ε = 20.7), dimethylsulfoxide (ε = 46.7), and water (ε = 78.4). The electronic energies were corrected with zero-point energies in the gas phase calculated at the B3LYP/6-31+G(d) level for the neutral and anionic forms. Electron affinity (*EA*) of PQ was calculated by subtracting the corrected electronic energy (E_{elec}) of the anionic form from that of the neutral one. The redox potential (E^o) *versus* the standard hydrogen electrode (SHE) for one electron reduction of PQ was calculated using the equation:

$$E^o = EA - 4.43,$$

where the value of 4.43 eV is an estimate of the absolute potential of SHE.[58,59]

Normal mode frequencies and IR intensities were calculated at the B3LYP/6-31+G(d) level for the optimized geometries in the neutral and anionic forms. The calculated vibrational frequencies were scaled with a scaling factor of 0.9730 following our previous study of $PQ^{\bullet-}$ calculation,[17] in which the calculated frequency of the main CO band in the $PQ^{\bullet-}$ model having two H-bonds with water molecules (PQ-2H in this work, see below) was adjusted to 1479 cm^{-1}, the experimental frequency of Q_A^-. To decouple the H_2O bending vibrations from the C=O/C=C vibrations at 1700–1600 cm^{-1} in neutral PQ models, hydrogen atoms in water molecules were replaced with deuterium atoms.

Results

DFT calculations of PQ complexes H-bonded to water molecules

a. Optimized geometries and redox potentials. Fig. 2 shows the optimized geometries of the neutral forms of H-bonded PQ models. PQ-1, which has a truncated isoprenoid chain, was used as a PQ model instead of PQ-9, which actually functions in plants, to save the CPU time. Previous experimental and theoretical studies showed only a minor effect of the length of the isoprenoid chain on the redox potential of PQ.[40,60] In addition to free PQ (Fig. 2a), four PQ complexes H-bonded to one to four water molecules at the C=O groups were subjected to calculations: PQ with one H-bond at C(4)=O (PQ-1H; Fig. 2b), PQ with two H-bonds (one H-bond at each C=O) (PQ-2H; Fig. 2c), PQ with three H-bonds (two H-bonds at C(1)=O and one H-bond at C(4)=O) (PQ-3H; Fig. 2d), and PQ with four H-bonds (two H-bonds at each C=O) (PQ-4H; Fig. 2e). PQ-2H and PQ-3H were used as H-bonded PQ models in our previous study to calculate the CO vibrations of their radical anions.[17] Geometry optimization of the semiquinone radicals of the corresponding complexes (Fig. S1 in the ESI†) exhibited no change in the H-bonding structures except for slightly altered orientations of water molecules.

The lengths of the CO and CC bonds in the PQ ring of the optimized structures in the neutral and anionic forms are summarized in Table 1. The following tendency of the effects of H-bonds was obtained in the neutral forms. (1) Upon formation of one H-bond to a C=O group (C(4)O of PQ-1H, PQ-2H, and PQ-3H, and C(1)O of PQ-2H), the CO length increases by +0.003–+0.006 Å. (2) Upon formation of two H-bonds to a single C=O group (C(1)O of PQ-3H and PQ-4H, and C(4)O of PQ-4H), the CO length increases by +0.008–+0.010 Å, *i.e.*, two times more than the case of a single H-bond. (3) The length of the C(2)=C(3) bond slightly increases (+0.001–+0.002 Å) upon formation of H-bond(s) to the C=O group(s).

Upon formation of semiquinone radical anions, the lengths of both the C(1)=O and C(4)=O bonds increased by +0.042–+0.049 Å, while those of the C(2)=C(3) and C(5)=C(6) bonds were lengthened by +0.025–+0.028 Å. Even in radical anions, the changes in the CO lengths by H-bond formation are similar to those of the neutral forms.

Table 2 summarizes the electronic energies (E_{elec}) of PQ and $PQ^{\bullet-}$ calculated in the gas phase and in various solvents with different ε values. The ε dependence of E_{elec} corrected with zero-point energies of PQ and $PQ^{\bullet-}$ is depicted in Fig. 3A. The E_{elec} of the $PQ^{\bullet-}$ anion is highly dependent on ε, whereas the E_{elec} of neutral PQ is rather insensitive to ε. The electron affinity (*EA*) and the redox potential *versus* SHE (E^o) estimated from the E_{elec} values of PQ and $PQ^{\bullet-}$ at different ε are also presented in Table 2, and the ε dependence of E^o is depicted in Fig. 3B. The E^o was estimated to be −2.545 V in the gas phase (ε = 1.0) but increased with larger ε to converge into a constant value of ∼−0.6 V.

Table 3 summarizes the E^o of the H-bonded PQ models calculated at various ε values. The data at ε = 4.9, which is close to the general ε value in proteins (ε = 4),[61,62] are selected to present a graph as a function of the number of H-bonds in Fig. 4. There is a linear relationship between E^o and the number of H-bonds, with a higher E^o with more H-bonds. The slope of the regression line provides the E^o change per H-bond. It is +172 meV/H-bond at ε = 4.9, and the slope becomes smaller at higher ε (Table 3).

b. Calculation of molecular vibrations. Fig. 5 shows calculated normal mode frequencies with IR intensities (red bars) in the C=O and C=C regions of the model PQ complexes in the neutral forms. IR spectra are also produced assuming Gaussian bands with a full width at half maximum of 8 cm^{-1} (black lines). There are four C=O/C=C stretching (νCO/νCC) modes of the PQ ring in this region. A weak C=C stretching band of the isoprenoid chain calculated at 1692–1689 cm^{-1} will not be discussed here. The asymmetric C=C stretching vibration (ν_{as}CC) is isolated at 1615–1611 cm^{-1}, while the other three vibrations are strongly coupled with each other.

The band patterns of the three νCO/νCC modes are different depending on the symmetry of the H-bonding structures. The PQ models with symmetric H-bonding structures (PQ, PQ-2H, and PQ-4H; Fig. 2a, c and e, respectively) showed a single strong band due mainly to the asymmetric C=O stretching vibration (ν_{as}CO). The corresponding symmetric C=O stretching vibration (ν_sCO) is coupled with the symmetric C=C stretching vibration (ν_sCC) and splits into two modes showing peaks on

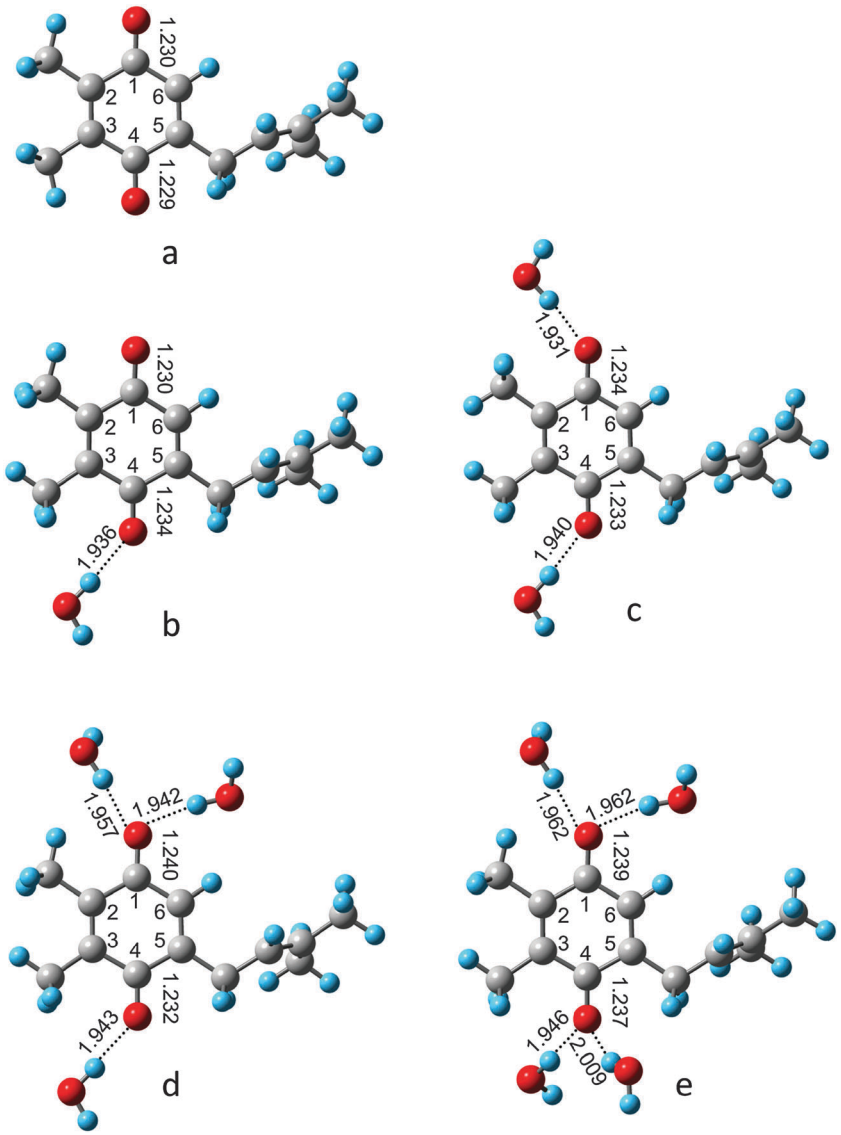

Fig. 2 Optimized geometries of the PQ model and its H-bonded complexes with water molecules in the neutral forms. (a) PQ: free plastoquinone-1, (b) PQ-1H: PQ with one H-bond at C(4)═O, (c) PQ-2H: PQ with two H-bonds (one H-bond at each C═O), (d) PQ-3H: PQ with three H-bonds (two H-bonds at C(1)═O and one H-bond at C(4)═O), and (e) PQ-4H: PQ with four H-bonds (two H-bonds at each C═O). Carbon, oxygen and hydrogen atoms are expressed as gray, red, and cyan balls, respectively.

the higher- and lower-frequency sides of the strong ν_{as}CO band. These modes generally have only weak IR intensities due to the symmetric motions of IR-active CO vibrations. The frequency of the ν_{as}CO mode decreases from 1666 cm^{-1} in free PQ to 1653 ($\Delta\nu$ = −13 cm^{-1}) and 1634 ($\Delta\nu$ = −32 cm^{-1}) cm^{-1} in PQ-2H and PQ-4H, respectively. Thus, in the symmetric H-bonded complexes, the typical band pattern is a single strong ν_{as}CO band at 1670–1630 cm^{-1} with a relatively weak ν_{as}CC band at ∼1615 cm^{-1}.

In contrast, the PQ models with asymmetric H-bonding structures (PQ-1H, and PQ-3H; Fig. 2b and d, respectively) have split νCO peaks (Fig. 5) by decoupling of the two C═O vibrations due to the different H-bond intensities and the resultant different C═O lengths (Table 1). In PQ-1H, all the three vibrational modes showed medium or strong intensities (Fig. 5b). The H-bonded C(4)═O bond has the lowest νCO frequency of 1644 cm^{-1}, while the νC(1)O mode has a higher frequency of 1673 cm^{-1}. The strongest peak at 1659 cm^{-1} is a coupled mode of ν_{as}CO and ν_{s}CC. In PQ-3H, the νC(1)O and νC(4)O modes separately appear at 1628 and 1652 cm^{-1} (Fig. 5d). The remaining mode of coupled ν_{s}CC and ν_{s}CO vibrations has only a weak intensity at a higher frequency of 1671 cm^{-1}.

The calculated νCO/νCC modes of semiquinone anion forms are shown in Fig. 6. The frequencies are calculated at 1520–1400 cm^{-1}, which is ∼200 cm^{-1} lower than the νCO/νCC region of the neutral forms, reflecting the lengthened CO and CC bonds (Table 1). The νCO and νCC vibrations are strongly coupled with the deformation vibrations of the Me groups (δMe) in the PQ ring. In all the PQ models, a strongest band mainly arising from the νCO vibration is observed in a narrow range of 1482–1474 cm^{-1}. Around this prominent band, mostly

Table 1 Calculated C═O and C═C bond lengths (Å) of PQ in the neutral and semiquinone anion forms and the effects of H-bonds with water molecules

		PQ model[a]				
		PQ	PQ-1H	PQ-2H	PQ-3H	PQ-4H
H-bonding structure		None	C(4)O···H	C(1)O···H C(4)O···H	C(1)O···2H C(4)O···H	C(1)O···2H C(4)O···2H
Neutral form						
C(1)O	*r*CO	1.230	1.230	1.234	1.240	1.239
	$\Delta r_{\text{H-bond}}$[b]	—	0.000	+0.004	+0.010	+0.009
C(4)O	*r*CO	1.229	1.234	1.235	1.232	1.237
	$\Delta r_{\text{H-bond}}$	—	+0.005	+0.006	+0.003	+0.008
C(2)C(3)	*r*CC	1.358	1.359	1.361	1.360	1.360
	$\Delta r_{\text{H-bond}}$	—	+0.001	+0.003	+0.002	+0.002
C(5)C(6)	*r*CC	1.346	1.346	1.345	1.347	1.347
	$\Delta r_{\text{H-bond}}$	—	0.000	−0.001	+0.001	+0.001
Semiquinone anion form						
C(1)O	*r*CO	1.274	1.272	1.278	1.286	1.283
	$\Delta r_{\text{H-bond}}$	—	−0.002	+0.004	+0.012	+0.009
	Δr_{anion}[c]	+0.044	+0.042	+0.044	+0.046	+0.044
C(4)O	*r*CO	1.275	1.283	1.279	1.277	1.284
	$\Delta r_{\text{H-bond}}$	—	+0.008	+0.004	+0.002	+0.009
	Δr_{anion}	+0.046	+0.049	+0.044	+0.045	+0.047
C(2)C(3)	*r*CC	1.385	1.385	1.386	1.386	1.385
	$\Delta r_{\text{H-bond}}$	—	0.000	+0.001	+0.001	0.000
	Δr_{anion}	+0.027	+0.026	+0.025	+0.026	+0.025
C(5)C(6)	*r*CC	1.374	1.373	1.372	1.372	1.372
	$\Delta r_{\text{H-bond}}$	—	−0.001	−0.002	−0.002	−0.002
	Δr_{anion}	+0.028	+0.027	+0.027	+0.025	+0.025

[a] Optimized geometries of model PQ complexes are shown in Fig. 2. [b] The change in the bond length by H-bond formation. [c] The change in the bond length by semiquinone anion formation.

Table 2 Calculated electronic energies, electron affinities, and redox potentials of PQ at various dielectric constants

	E_{elec}[b] (eV)			
ε[a]	PQ	$PQ^{\bullet-}$	*EA*[c] (eV)	E^{o}[d] (V)
1.0	−17 834.547	−17 836.432	1.885	−2.545
1.4	−17 834.595	−17 837.034	2.439	−1.991
2.2	−17 834.647	−17 837.583	2.936	−1.494
4.9	−17 834.706	−17 838.100	3.394	−1.036
10.4	−17 834.742	−17 838.373	3.631	−0.799
20.7	−17 834.760	−17 838.497	3.737	−0.693
46.7	−17 834.770	−17 838.567	3.797	−0.633
78.4	−17 834.774	−17 838.589	3.815	−0.615

[a] Dielectric constants of the gas phase (1.0), argon (1.4), benzene (2,2), chloroform (4.9), dichloroethane (10.4), acetone (20.7), dimethylsulfoxide (46.7), and water (78.4). [b] Electronic energies corrected with zero-point energies of PQ and $PQ^{\bullet-}$ were calculated at the B3LYP/6-311+G(3df,3pd) level after geometry optimization at the B3LYP/6-31+G(d) level. [c] Electron affinity obtained as a difference between the E_{elec} values of PQ and $PQ^{\bullet-}$. [d] Redox potential *vs.* SHE of the PQ/$PQ^{\bullet-}$ redox couple calculated by $E^{o} = EA - 4.43$.

on the lower frequency side (1470–1450 cm^{-1}), a bunch of bands with medium or weak intensities arising from the coupled νCO, νCC and δMe vibrations exist. At a higher frequency of 1516–1502 cm^{-1}, a weak band of the coupled ν_{as}CC, δMe and δCH vibrations appears, while at a lower frequency of 1420–1405 cm^{-1}, there is a band due to the stretching vibrations of the CC single bonds (C(2)–C(1)–C(6) and C(3)–C(4)–C(5)) coupled with the δMe vibrations.

DFT calculations of PQ complexes mimicking Q_A and Q_B interactions in PSII

PQ complexes mimicking the H-bonding interactions of Q_A and Q_B in PSII (Fig. 1A) were constructed using simple amino-acid models (Fig. 7 and Fig. S2, ESI†). In the Q_A model (Fig. 7a), 4-methylimidazole as a model of the D2-H214 side chain and *N*-methylacetamide as a model of the D2-A260 backbone amide interact with C(1)═O and C(4)═O, respectively. D2-T217, whose oxygen atom is located at 3.8 Å away from the C(1)═O in the X-ray structure (Fig. 1A),[22] was not involved in the H-bonded complex. In the Q_B model (Fig. 7b), the OH and NH groups of HO–$(CH_2)_2$–CONH–CH_3, which mimics the D1-S264 side chain and the D1-F265 backbone amide, interact with C(1)═O, and the NH of 4-methylimidazole as a model of D1-H215 interacts with C(4)═O. Thus, the Q_A model has two H-bonds, one at C(1)═O with imidazole NH and the other at C(4)═O with amide NH, while the Q_B model has three H-bonds, two at C(1)═O with alcohol OH and amide NH and one at C(4)═O with imidazole NH. The H-bonding patterns of the Q_A and Q_B models are the same as those of PQ-2H and PQ-3H, respectively.

The calculated CO and CC bond lengths of PQ in these model complexes are summarized in Table 4. The tendency of the changes in the bond lengths by H-bond formation and semiquinone anion formation in the Q_A and Q_B models is very similar to that in PQ-2H and PQ-3H, respectively. The E_{elec}, *EA*, and E^{o} values of the Q_A and Q_B models calculated at ε = 4.9 are presented in Table 5, and the E^{o} values are plotted in Fig. 4 (red circles) in comparison with other complexes with water

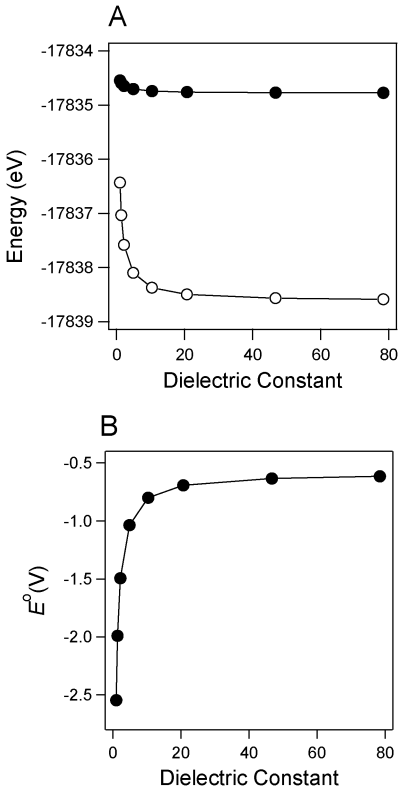

Fig. 3 (A) Calculated electronic energies of PQ in the neutral (closed circles) and semiquinone anion (open circles) forms as a function of dielectric constant. Electronic energies were corrected with zero-point energies calculated for the neutral and anionic forms in the gas phase. (B) Calculated redox potential of the PQ/PQ$^{\bullet-}$ redox couple as a function of dielectric constant.

Table 3 Calculated redox potentials (V) of model PQ complexes H-bonded to water molecules at various dielectric constants

	$E^{o\,b}$ (V)					
ε^a	PQ	PQ-1H	PQ-2H	PQ-3H	PQ-4H	ΔE^o/H-bond^c (mV)
1.0	−2.545	−2.242	−1.936	−1.651	−1.438	+281
1.4	−1.991	−1.726	−1.464	−1.210	−1.026	+245
2.2	−1.494	−1.265	−1.043	−0.824	−0.671	+209
4.9	−1.036	−0.842	−0.657	−0.478	−0.359	+172
10.4	−0.799	−0.624	−0.458	−0.305	−0.206	+151
20.7	−0.693	−0.525	−0.369	−0.228	−0.138	+141
46.7	−0.633	−0.471	−0.320	−0.186	−0.102	+135
78.4	−0.615	−0.454	−0.304	−0.173	−0.090	+133

^{a} Dielectric constants of the gas phase (1.0), argon (1.4), benzene (2,2), chloroform (4.9), dichloroethane (10.4), acetone (20.7), dimethylsulfoxide (46.7), and water (78.4). ^{b} The structures of the model PQ complexes are presented in Fig. 2. ^{c} The E^o change for one H-bond increase was estimated as a slope of the regression line.

molecules. The calculated E^o values of Q_A (−556 mV) and Q_B (−444 mV) models are in fair agreement with those of PQ-2H (−657 mV) and PQ-3H (−478 mV), respectively, although the former models H-bonded to amino acids have a little higher value. The E^o difference of 112 mV between the former two models is comparable to that of 172 mV between the latter two models.

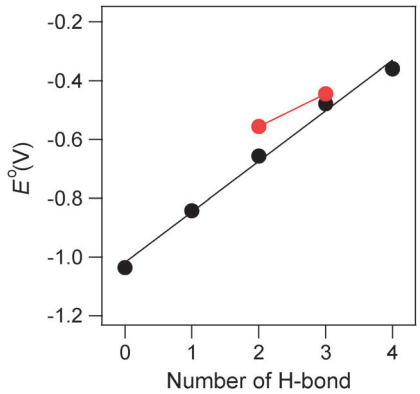

Fig. 4 H-bond number dependence of the calculated redox potentials of the PQ complexes with different H-bonding interactions. Black circles: free PQ and the H-bonded complexes with water molecules. Red circles: PQ complexes H-bonded to amino acid models. The redox potentials were calculated at a dielectric constant of 4.9.

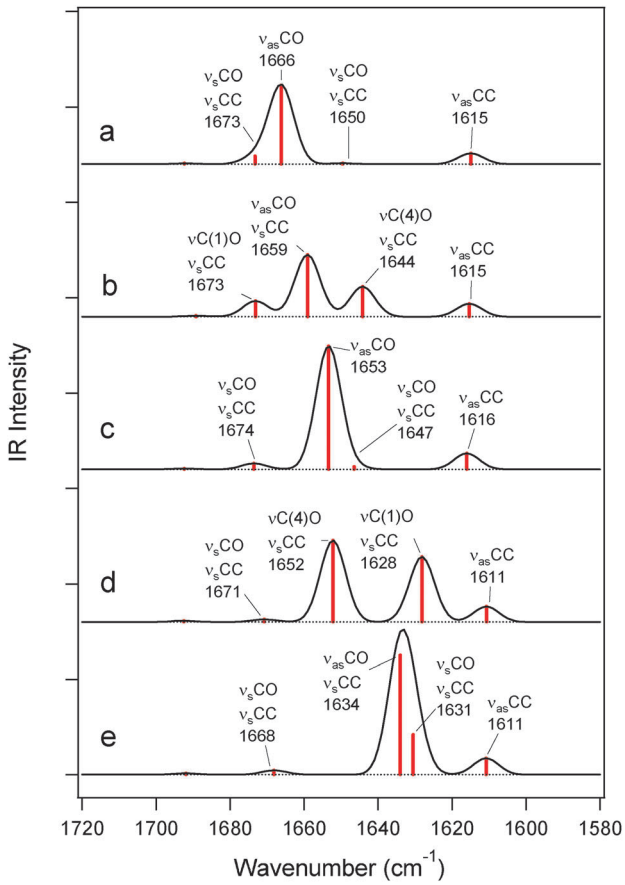

Fig. 5 Calculated IR spectra in the CO/CC stretching region of free PQ and the PQ complexes H-bonded to water molecules in the neutral forms. (a) PQ, (b) PQ-1H, (c) PQ-2H, (d) PQ-3H, and (e) PQ-4H. The calculated vibrational frequencies, which were scaled with a factor of 0.9730, are shown in red bars. Spectra were produced with Gaussian bands with a width (FWHM) of 8 cm^{-1}. The scale of IR intensity is 500 km mol^{-1} for a division.

Calculated IR spectra in the C=O/C=C region of the neutral forms of the Q_A and Q_B models are shown in Fig. 8. Except for

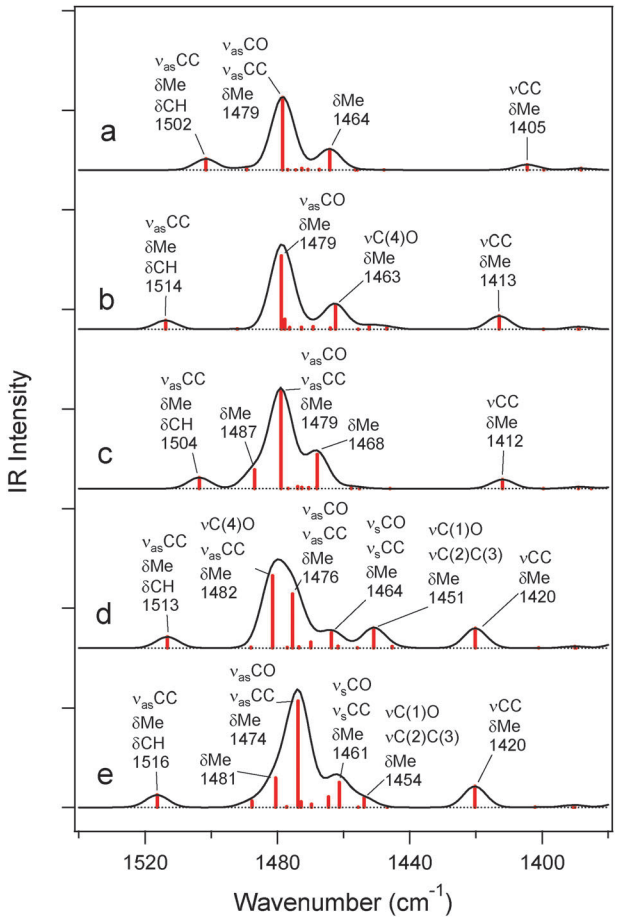

Fig. 6 Calculated IR spectra in the CO/CC stretching region of free PQ and the PQ complexes H-bonded to water molecules in the radical anion forms. (a) PQ, (b) PQ-1H, (c) PQ-2H, (d) PQ-3H, and (e) PQ-4H. The calculated vibrational frequencies, which were scaled with a factor of 0.9730, are shown in red bars. Spectra were produced with Gaussian bands with a width (FWHM) of 8 cm^{-1}. The scale of IR intensity is 500 km mol^{-1} for a division.

the additional band of the H-bonded amide (CO stretch + NH bend) at 1710–1680 cm^{-1}, band features of the PQ vibrations of the Q_A and Q_B models are very similar to those of PQ-2H (Fig. 5c) and PQ-3H (Fig. 5d), respectively. In the Q_A model, one strong ν_{as}CO band appears at 1656 cm^{-1} with weak side bands due to the coupled ν_sCO/ν_sCC vibrations. The lower-frequency side band at 1641 cm^{-1} gained a slightly larger intensity than the corresponding band at 1647 cm^{-1} in PQ-2H, reflecting the asymmetry in the H-bonding partners (imidazole NH and amide NH) at C(1)═O and C(4)═O. In the Q_B model, C═O vibrations split into two strong bands of the C(4)═O and C(1)═O modes at 1655 and 1638 cm^{-1}, respectively.

The calculated IR spectra in the νCO/νCC region of the semiquinone anions of the Q_A and Q_B models are shown in Fig. 9 (red bars and black lines). The spectral features with one strong band near 1480 cm^{-1} due mainly to the νCO vibration surrounded by medium- or weak-intensity bands, mostly on the lower-frequency side, are similar to the calculated IR spectra of PQ-2H and PQ-3H (Fig. 6c and d). In the Q_A and Q_B models, however, the number of modes in this region is much more than that of PQ-2H and PQ-3H (22 and 23 normal modes in the Q_A and Q_B models, respectively, *versus* 13 normal modes in PQ-2H and PQ-3H between 1520 and 1410 cm^{-1}) and the PQ modes are complexly mixed with the vibrations of H-bonding amino acid groups. Typically, the PQ vibrations in the Q_A model are coupled with the δNH, δCH, and νCN vibrations of imidazole, while those in the Q_B model are coupled with the δOH and δCH_2 vibrations of the Ser side chain in addition to the imidazole vibrations (Fig. 9).

In Fig. 9, the calculated spectra (black lines) are also compared with the experimental Q_A^--minus-Q_A and Q_B^--minus-Q_B spectra (blue lines) of PSII core complexes from *Thermosynechococcus elongatus* reported previously.[32] Note that in the experimental spectra, prominent amide I (1700–1600 cm^{-1}) and amide II (~1550 cm^{-1}) bands of protein backbones[31,32] do not interfere with the νCO/νCC region of a semiquinone anion, whereas amide I bands severely overlap the νCO/νCC region of the neutral PQ (1700–1600 cm^{-1}; Fig. 5 and 8). It is shown that the characteristics of the experimental Q_A^- and Q_B^- spectra were well reproduced by calculations. There is a major strong νCO band at ~1480 cm^{-1} together with a complex feature on the lower-frequency side. The latter complex feature is in agreement with the presence of numerous bands in the calculated spectra arising from the couplings of the PQ vibrations with the H-bonding amino acid vibrations.

Discussion

Redox potentials of the PQ models

The present DFT calculation estimated the *EA* of free PQ in the gas phase to be 1.885 eV, which agrees well with the experimental EAs of various quinones such as benzoquinone (1.9 eV), 2,5-dimethyl-benzoquinone (1.8 eV), and 2,3,5,6-tetramethyl-benzoquinone (1.6 eV),[63–65] confirming an appropriate level of calculation used in this study. However, the calculated E^o of PQ upon semiquinone anion formation in the gas phase, −2.545 V, was much lower than the experimental E_m of PQ-9, which has been estimated to be −0.3 to −0.4 V *vs.* SHE in *N*,*N*-dimethylformamide[60] and acetonitrile.[66] Because E^o for one-electron reduction or oxidation of a compound is generally affected by the ε of a medium,[41,67] we have calculated the E^o of PQ in various solvents using IEF-PCM approximation (Fig. 3B and Table 2). It was shown that E^o is highly dependent on the ε of solvent especially at relatively low ε ($\varepsilon < 10$); the E^o steeply increases as ε increases and converges into a constant value at a high enough ε. The E^o of free PQ was estimated to be −0.633 to −0.693 V at ε = 20.7–46.7 near the dielectric constants of *N*,*N*-dimethylformamide (ε = 38) and acetonitrile (ε = 37.5) (Table 3). These values are much closer to the experimental ones but still lower by ~0.3 V. Thus, absolute E^o values calculated in the polarizable continuum model for solvent interactions do not reproduce enough the experimental values. This might be partly related to the experimental fact that E_m of quinones are not directly related to the ε values of solvents but rather correlated with the acceptor numbers,[68,69] indicating that local quinone–solvent interactions represented by H-bonding interactions are important for E^o values.

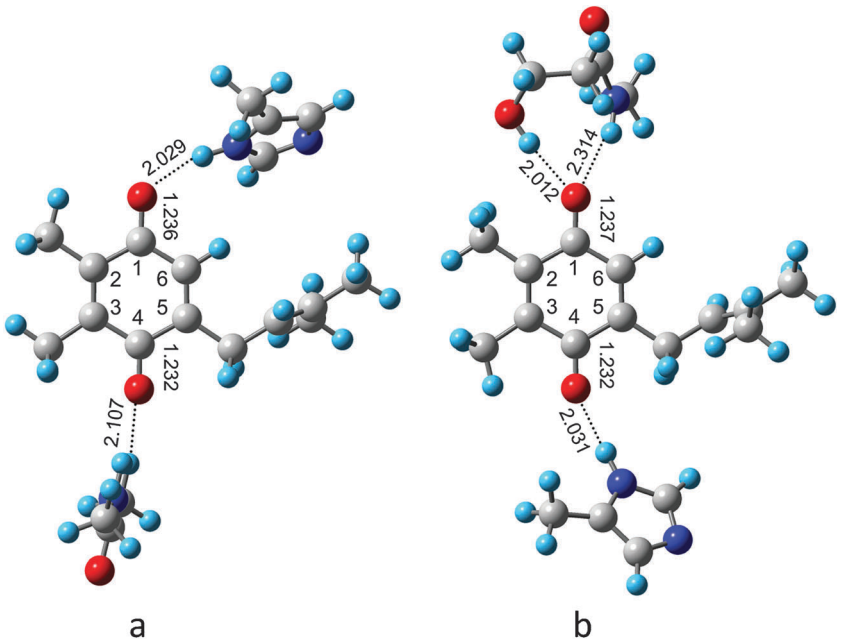

Fig. 7 Optimized geometries of the neutral forms of PQ complexes H-bonded to amino acid models mimicking the Q_A ((a) Q_A model) and Q_B ((b) Q_B model) interactions in PSII. In the Q_A model (a), C(1)═O and C(4)═O interact with 4-methylimidazole as a model of the D2-His214 side chain and *N*-methylacetamide as a model of the D2-A260 backbone amide, respectively. In the Q_B model (b), C(1)═O interacts with the OH and NH groups of HO–$(CH_2)_2$–CONH–CH_3 that mimics the D1-S264 side chain and the D1-F265 backbone amide, while C(4)═O interacts with 4-methylimidazole as a model of the D1-His215 side chain. Carbon, oxygen, nitrogen, and hydrogen atoms are expressed as gray, red, blue, and cyan balls, respectively.

Table 4 Calculated C═C and C═O bond lengths (Å) of the neutral and semiquinone anion forms of PQ complexes H-bonded to amino acid models mimicking Q_A and Q_B interactions in PSII

		PQ model[a]	
		Q_A model	Q_B model
H-bonding structure		C(1)O···H C(4)O···H	C(1)O···2H C(4)O···H
Neutral form			
C(1)O	*r*CO	1.236	1.237
	$\Delta r_{\text{H-bond}}$[b]	+0.006	+0.007
C(4)O	*r*CO	1.232	1.232
	$\Delta r_{\text{H-bond}}$	+0.003	+0.003
C(2)C(3)	*r*CC	1.358	1.359
	$\Delta r_{\text{H-bond}}$	0.000	+0.001
C(5)C(6)	*r*CC	1.347	1.346
	$\Delta r_{\text{H-bond}}$	+0.001	0.000
Semiquinone anion form			
C(1)O	*r*CO	1.282	1.286
	$\Delta r_{\text{H-bond}}$	+0.008	+0.012
	Δr_{anion}[c]	+0.046	+0.049
C(4)O	*r*CO	1.279	1.278
	$\Delta r_{\text{H-bond}}$	+0.004	+0.003
	Δr_{anion}	+0.047	+0.046
C(2)C(3)	*r*CC	1.384	1.385
	$\Delta r_{\text{H-bond}}$	−0.001	0.000
	Δr_{anion}	+0.026	+0.026
C(5)C(6)	*r*CC	1.373	1.372
	$\Delta r_{\text{H-bond}}$	−0.001	−0.002
	Δr_{anion}	+0.026	+0.026

[a] Optimized geometries of model PQ complexes are shown in Fig. 7. [b] The change in the bond length by H-bond formation. [c] The change in the bond length by semiquinone anion formation.

Table 5 Calculated electronic energies, electron affinities, and redox potentials of PQ complexes H-bonded to amino acid models mimicking Q_A and Q_B interactions in PSII

	E_{elec}[a] (eV)				
PQ model[b]	Neutral	Anion	*EA*[c] (eV)	E^{o}[d] (V)	ΔE^{o}[e] (mV)
Q_A model	−31 835.996	−31 839.870	3.874	−0.556	0
Q_B model	−34 953.708	−34 957.694	3.986	−0.444	+112

[a] Energies were calculated at a dielectric constant of 4.9. [b] The structures of the PQ complexes are shown in Fig. 7. [c] Electron affinity obtained as a difference between the E_{elec} values of neutral and semiquinone anion forms. [d] Redox potential *vs.* SHE calculated by $E_{\text{red}} = EA - 4.43$. [e] The difference in the calculated redox potential of the Q_A model.

To investigate the effect of H-bonding interactions on the E^{o} of PQ, we have calculated the E^{o} values of PQ models with various H-bonding structures, in which the number of H-bonds at the C═O group(s) with water molecule(s) is changed from one to four (Fig. 2). It was clearly shown that the PQ model with more H-bonds has a higher E^{o} value (Fig. 4 and Table 3). It is notable that E^{o} and the number of H-bonds have a linear relationship. This indicates that there is virtually no difference in the effects of H-bonding on E^{o} between the interactions at the C(1)═O and C(4)═O and between the first and second H-bonds at each C═O group. The slope of the regression line in the H-bond number dependence is smaller at higher ε; *e.g.*, +281, +172, and +133 mV for one H-bond increase at ε = 1, 4.9, and 78.9, respectively (Table 3). The calculated increase in E^{o} by H-bond formation is consistent with the previous experimental results.[70–73]

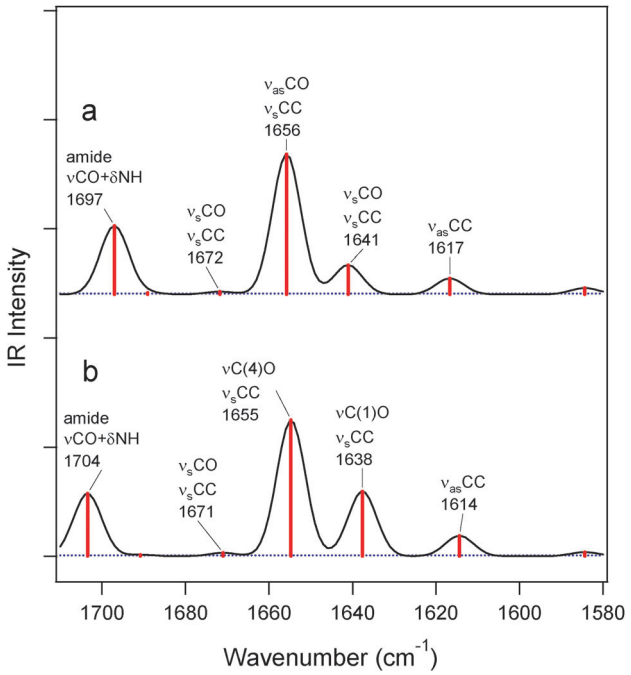

Fig. 8 Calculated IR spectra in the CO/CC stretching region of the Q_A (a) and Q_B (b) models in the neutral forms. The calculated vibrational frequencies, which were scaled with a factor of 0.9730, are shown in red bars. Spectra were produced with Gaussian bands with a width (FWHM) of 8 cm^{-1}. The scale of IR intensity is 500 km mol^{-1} for a division.

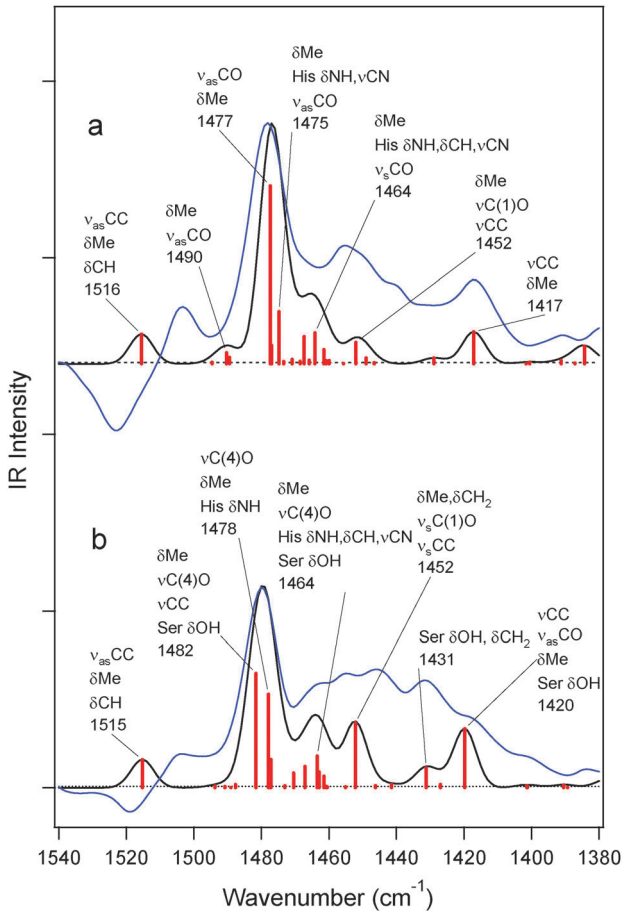

Fig. 9 Calculated IR spectra in the CO/CC stretching region of the Q_A (a) and Q_B (b) models in the semiquinone anion forms (black lines) in comparison with experimental spectra of Q_A^- and Q_B^- (blue lines). The calculated vibrational frequencies, which were scaled with a factor of 0.9730, are shown in red bars. Spectra were produced with Gaussian bands with a width (FWHM) of 8 cm^{-1}. The scale of IR intensity is 500 km mol^{-1} for a division. Experimental spectra were taken from the Q_A^--minus-Q_A and Q_B^--minus-Q_B FTIR difference spectra of PSII core complexes from *Thermosynechococcus elongatus*[32] and were scaled so that the intensities of the strongest CO bands were adjusted to those of the calculated spectra.

For example, Feldman *et al.*[72] showed that phylloquinone derivatives increased the E_m by 70–240 mV by forming an intramolecular H-bond, while Coates *et al.*[73] reported that the E_m of naphthoquinone derivatives increased by 200–300 mV by changing a solvent from aprotic acetonitrile to protic ethanol. Previous calculations are also consistent with our calculations, showing increases in *EA* or E^o of quinones by H-bond formation.[37,39,41]

The Q_A and Q_B models (Fig. 7), which have H-bonding partners of amino acid models mimicking the interactions in PSII proteins, showed E^o values similar to those of PQ-2H and PQ-3H (Fig. 2c and d), respectively, which have the same H-bonding structures but with water molecules. The calculated E^o values are −556 and −444 mV for the Q_A and Q_B models, respectively, at $\varepsilon = 4.9$, while the corresponding E^o values are −657 and −478 mV for PQ-2H and PQ-3H, respectively (Fig. 4, Tables 3 and 5). The E^o increase from the Q_A to the Q_B models is +112 mV, which is comparable with +179 mV from PQ-2H to PQ-3H (or +172 mV/H-bond as the slope of the regression line in Fig. 4). This calculation result indicates that the number of H-bonds is an important factor to determine the E^o value, although the difference in the chemical species of the H-bonding partners may also have some effect.

The calculated E^o of the simple Q_A model (−556 mV) could not well reproduce the experimental E_m value of Q_A, −80 mV.[8] This result suggests that the protein environments around Q_A, especially the electrostatic interactions with the protein moieties,[16] are significant in determining the absolute E_m value. In contrast, the experimental E_m gap between Q_A and Q_B, which has been estimated to be ∼+80 mV,[9,10] is comparable to the E^o difference between the Q_A and Q_B models (+112 mV) obtained by DFT calculations, suggesting that an additional H-bond from the D1-Ser264 OH to Q_B is an important factor for the E_m gap. This is consistent with previous calculations of the E_m values of Q_A and Q_B based on the linearized Poisson–Boltzmann equation,[16] in which the ΔE_m ($Q_B - Q_A$) was estimated to be +53–86 mV and the $E_m(Q_B)$ decreased by 132–165 mV upon removal of a H-bond of D1-Ser264.

Calculated IR spectra: criteria for the H-bonding structure of PQ

a. Neutral forms of PQ complexes. The H-bonding structures of quinones are reflected in IR spectra, especially in the CO stretching bands.[17,44,47,48,50] Hence, it is important to provide clear criteria for interpretation of the CO bands to determine the H-bonding structure of PQ. In the neutral forms of the PQ complexes H-bonded to water molecules, one strong C═O

band arising from the ν_{as}CO vibration appears when they have symmetric H-bonding interactions such as free PQ, PQ-2H, and PQ-4H, whereas two prominent bands with main contributions from individual C(1)═O and C(4)═O vibrations appear in the PQ complexes with asymmetric H-bonding interactions like PQ-1H and PQ-3H (Fig. 5). In PQ-2H and PQ-4H, the ν_{as}CO frequency is lower than that of free PQ by 13 and 33 cm^{-1}, respectively, by formation of one and two H-bonds at each C═O. Also, PQ-1H with a single H-bond at C(4)═O has a νC(4)O frequency lower by 29 and 15 cm^{-1} than the νC(1)O and ν_{as}CO frequencies, respectively, while in PQ-3H, the νC(1)═O with two H-bonds has a νCO frequency lower by 24 cm^{-1} than the νC(4)═O with one H-bond. The presence of a single strong C═O band in free or symmetrically H-bonded PQ is in agreement with the experimental IR spectra in aprotic and protic solvents.[31,46,74,75] The splitting of C═O bands by asymmetric H-bonding interactions with PQ was also pointed out previously by Bandaranayake *et al.*[48] by DFT calculations for the PQ model singly H-bonded at C(4)═O. Thus, a single prominent C═O band or split C═O bands as well as their frequencies can be good criteria for determining the symmetry of the H-bonded structure and the number of H-bonds.

These criteria basically hold in the Q_A and Q_B models. The Q_A model has symmetric H-bonding interactions but with different H-bonding partners (imidazole and amide; Fig. 7a), while the Q_B model has asymmetric H-bonding interactions (Fig. 7b). The band patterns of the Q_A and Q_B models (Fig. 8) were similar to those of PQ-2H and PQ-3H, respectively. Thus, the difference in the H-bonding partners in the Q_A model is not much sensitive to the band feature of the C═O vibrations, although a slight intensity increase in the ν_sCO band at 1641 cm^{-1} on the lower frequency side of the main peak seems to reflect the asymmetry in the H-bonding partners.

Although the dependence of the C═O vibrations on the H-bonding structure in the neutral PQ forms is now clear, the C═O region (1700–1600 cm^{-1}) of neutral PQ in the Q_A^--minus-Q_A and Q_B^--minus-Q_B difference spectra severely overlap strong, complex bands of amide I vibrations arising from the perturbations of protein backbones upon Q_A^- and Q_B^- formation.[31,32] Thus, replacement of Q_A and Q_B with isotope labeled PQ is necessary to identify the C═O bands of the neutral forms. Such isotope substitution studies using $^{13}C/^{18}O$ labeled quinones have been performed in bacterial reaction centers[27–29] and PSI,[34] but have not yet been reported in PSII.

b. Semiquinone anion forms of PQ complexes. The semiquinone anion forms of PQ complexes show the νCO/νCC frequencies lower by ~200 cm^{-1} than those of the neutral forms due to significantly lengthened C═O and C═C bonds in the quinone ring (Tables 1 and 4), which originate from the antibonding character of the singly occupied molecular orbital of the semiquinone radical anion.[42,76] All the H-bonded complexes showed a similar spectral pattern of a single strong band near 1480 cm^{-1}, which arises from the ν_{as}CO vibration coupled with the ν_{as}CC and δMe vibrations, surrounded by numerous weak or medium bands due to complex couplings of νCO, νCC, δMe, and δCH vibrations (Fig. 6). The frequency of the main band is not very sensitive to the H-bonded structures (Fig. 6) in contrast to the neutral forms, and is found only in a narrow range (1479 ± 5 cm^{-1}). The direction of shift does not show a clear tendency, and also there is no clear pattern in the side bands except that more H-bonded complexes seem to have more complex band features. These properties of the bands in the νCO region of the semiquinone anion is ascribed to the lower contribution of the νCO vibrations to the normal modes due to strong couplings with other vibrations, which originally have nearby frequencies, such as δMe, δCH and single bond νC–C vibrations. Indeed, the potential energy distribution of the νCO vibrations in the main νCO mode at 1479 cm^{-1} of free PQ in the anionic form was only 57%, in contrast to 83% in the νCO mode at 1666 cm^{-1} in the neutral form.

In the Q_A and Q_B models (Fig. 7), the bands are further coupled with amino acid vibrations such as the NH and OH bending vibrations of His and Ser side chains, respectively, providing more complex features with a larger number of vibrational modes than the PQ complexes with water molecules (Fig. 9). The calculated band features fairly reproduced the experimental spectra of Q_A^- and Q_B^- in the Q_A^--minus-Q_A and Q_B^--minus-Q_B FTIR difference spectra (Fig. 9).[32] However, the intensities of the board features at 1470–1400 cm^{-1} on the lower frequency side of the major strong band are larger in the experimental Q_A^- and Q_B^- spectra than the calculated spectra. Our Q_A and Q_B models adopted the simplest amino acid structures as H-bonding partners (Fig. 7). Stronger intensities of the experimental bands might imply a larger number of couplings with the vibrations from protein moieties in real Q_A and Q_B in PSII. Although the Q_A and Q_B models with two and three H-bonds, respectively, are consistent with experimental spectra, no definite evidence was obtained from the anion CO bands for approving the H-bonding structure predicted from the X-ray structure.[22] Nevertheless, due to significant couplings of the H-bonding amino acid vibrations with the νCO vibrations of the PQ radical anion, the complex spectral features in this region (Fig. 9) are useful to monitor the interaction changes of Q_A and Q_B in PSII proteins upon certain treatments.

E_m Changes of Q_A by Mn depletion and herbicide binding

It has been known that the E_m of Q_A increases by ~140 mV by depletion of the Mn_4Ca cluster or even depletion of only Ca^{2+} in the cluster.[8,11] The E_m increase of Q_A makes the E_m gap between Q_A and Q_B smaller and that between Pheo and Q_A larger, and hence relaxation of Q_B^- through Q_A is promoted whereas reverse electron transfer from Q_A^- to Pheo leading to the formation of a harmful triplet state is suppressed.[13,14] Thus, the E_m control of Q_A by Mn_4Ca depletion is proposed to be one of the photoprotection mechanisms that PSII evolved.[13,14] Ishikita *et al.*[16] suggested based on linearized Poisson–Boltzmann calculations that H-bonding by D2-Thr217 to the C(1)═O of Q_A upshifts the E_m by ~100 mV. This result is consistent with the present DFT calculation that an upshift of E^o by ~+100–200 mV is expected due to additional single H-bond formation. If this is the case, some changes are expected to take place in the νCO/νCC region of the Q_A^- FTIR spectrum upon Mn_4Ca depletion.

However, the frequency of the strongest CO band at 1478–1479 cm^{-1} did not change at all between the $Q_A^-S_2$-minus-Q_AS_1 and Q_A^--minus-Q_A spectra in intact and Mn_4Ca-depleted PSII samples, respectively.[17] Also, a double difference spectrum between $Q_A^-S_2$-minus-Q_AS_1 (intact) and Q_A^--minus-Q_A (Mn_4Ca-depleted) difference spectra showed no specific feature in the 1500–1440 cm^{-1} region,[77] indicating that there is no spectral changes in this region by Mn_4Ca depletion. These observations suggest that there is no change at least in the H-bonding pattern in Q_A^- upon Mn_4Ca depletion. The possible mechanism of the E_m change by Mn_4Ca depletion is therefore that the H-bonding structure in neutral Q_A is changed or the H-bond strength is changed without a change in the basic H-bonding pattern.

Binding of a herbicide to the Q_B site affects the E_m of Q_A. The urea-type herbicide, DCMU, raises the $E_m(Q_A)$ by $\sim$50 mV, whereas phenolic herbicide, bromoxynil, lowers the $E_m(Q_A)$ by $\sim$45 mV.[12] Our previous FTIR study showed that urea, triazine, and uracil-type herbicides showing higher thermoluminescence temperatures (*i.e.*, higher E_m values) provided a slightly higher frequency by $\sim$1 cm^{-1} in the main CO peak of Q_A^- than phenolic herbicides showing lower thermoluminescence temperatures (*i.e.*, lower E_m values) without a specific difference in the band pattern.[17] This FTIR difference was interpreted to reflect the change in the H-bonding strength without changing the H-bonding pattern by comparison of the calculated IR spectra of PQ-2H, PQ-3H, and the PQ complex in which additional water is attached to the water of PQ-2H to increase the H-bonding intensity. The DFT calculations in this study with a more number of H-bonded models, showing the sensitivity of the H-bonding structure to the spectral features around the main CO peak, confirmed the conclusion that the H-bonding pattern is basically not changed by treatment of different herbicides. The influence of a strong H-bond of the phenolate anion of bromoxynil with D2-H215[78] on the H-bond between Q_A and D1-H214 through the His–Fe–His bridge (Fig. 1A) was suggested by theoretical calculations using DFT and Poisson–Boltzmann approaches.[19] Further FTIR analyses to study the effects of Mn_4Ca depletion and herbicide binding on the C=O bands of neutral Q_A will be fruitful in full understanding of the mechanism of the redox potential control of Q_A in PSII.

Conclusion

The present DFT calculations showed that the redox potential of PQ is highly dependent on its H-bonding interactions. Additional single H-bond formation to the C=O group of PQ upshifts the E^o value by 100–200 mV, which would provide a significant effect on the redox reactions of quinones in proteins. This H-bonding dependency of the quinone potential should hold for other types of quinone molecules that function in PSI and bacterial reaction centers. Thus, adding, removing, or changing the intensities of H-bonds to the quinone C=O groups may be a common strategy of potential control in quinone-binding proteins. In PSII, H-bonding interactions can be a key factor to generate the E_m gap between Q_A and Q_B and the E_m shifts of Q_A by treatments like Mn_4Ca depletion and herbicide binding, although detailed mechanisms remain to be clarified by further theoretical and experimental studies.

H-bonding interactions of quinones in proteins can be monitored by FTIR difference spectroscopy. Neutral forms show significant changes in the CO stretching vibrations at 1700–1600 cm^{-1}, which provide good criteria to determine the H-bonding structures. However, significant overlaps with strong amide I vibrations from protein backbones hamper clear assignments of CO bands and hence substitution experiments using $^{13}C/^{18}O$ isotope-labeled quinones are necessary. In contrast, assignment of the CO bands of a semiquinone anion in proteins is much easier because of large downshifts to 1500–1450 cm^{-1}, where there is no significant overlap with major protein bands. Although the present DFT calculations showed that the main CO peak of the semiquinone anion is not very sensitive to H-bonding interactions, the spectral features formed by numerous side bands, which arise from normal modes complexly coupled with other quinone vibrations and the vibrations of H-bonding amino acids, are useful monitors for detecting the changes in the H-bonding structure in proteins. Thus, the results in the present study showed that FTIR measurements combined with theoretical DFT calculations are useful methods for full understanding of the molecular mechanism of redox potential control of quinones in PSII and other photosynthetic proteins.

Acknowledgements

Computations were partly performed at Research Center for Computational Science, Okazaki, Japan. This study was supported by the Grants-in-Aid for Scientific Research from the Ministry of Education, Culture, Sports, Science and Technology (23657099, 24000018, 24107003, and 25291033).

References

1 G. Renger and A. R. Holzwarth, in *Photosystem II: The Light-Driven Water:Plastoquinone Oxidoreductase*, ed. T. Wydrzynski and K. Satoh, Springer, Dordrecht, The Netherlands, 2005, pp. 139–175.
2 B. A. Diner and F. Rappaport, *Annu. Rev. Plant Biol.*, 2002, **53**, 551–580.
3 W. Hillier and J. Messinger, in *Photosystem II: The Light-Driven Water:Plastoquinone Oxidoreductase*, ed. T.Wydrzynski and K.Satoh, Springer, Dordrecht, The Netherlands, 2005, pp. 567–608.
4 J. P. McEvoy and G. W. Brudvig, *Chem. Rev.*, 2006, **106**, 4455–4483.
5 J. Messinger, T. Noguchi and J. Yano, in *Molecular Solar Fuels*, ed. T. Wydrzynski and W. Hillier, Royal Society of Chemistry, Cambridge, U.K., 2012, ch. 7, pp. 163–207.
6 G. Renger, *Biochim. Biophys. Acta*, 2012, **1817**, 1164–1176.
7 V. Petrouleas and A. R. Crofts, in *Photosystem II: The Light-Driven Water:Plastoquinone Oxidoreductase*, ed. T. Wydrzynski

and K. Satoh, Springer, Dordrecht, The Netherlands, 2005, pp. 177–206.
8 A. Krieger, A. W. Rutherford and G. N. Johnson, *Biochim. Biophys. Acta*, 1995, **1229**, 193–201.
9 A. R. Crofts and C. A. Wraight, *Biochim. Biophys. Acta*, 1983, **726**, 149–185.
10 J. Minagawa, Y. Narusaka, Y. Inoue and K. Satoh, *Biochemistry*, 1999, **38**, 770–775.
11 G. N. Johnson, A. W. Rutherford and A. Krieger, *Biochim. Biophys. Acta*, 1995, **1229**, 202–207.
12 A. Krieger-Liszkay and A. W. Rutherford, *Biochemistry*, 1998, **37**, 17339–17344.
13 A. W. Rutherford and A. Krieger-Liszkay, *Trends Biochem. Sci.*, 2001, **26**, 648–653.
14 A. Krieger-Liszkay, C. Fufezan and A. Trebst, *Photosynth. Res.*, 2008, **98**, 551–564.
15 I. Idedan, T. Tomo and T. Noguchi, *Biochim. Biophys. Acta*, 2011, **1807**, 1214–1220.
16 H. Ishikita and E. W. Knapp, *J. Am. Chem. Soc.*, 2005, **127**, 14714–14720.
17 A. Takano, R. Takahashi, H. Suzuki and T. Noguchi, *Photosynth. Res.*, 2008, **98**, 159–167.
18 S. Rose, J. Minagawa, M. Seufferheld, S. Padden, B. Svensson, D. Kolling, A. Crofts and Govindjee, *Photosynth. Res.*, 2008, **98**, 449–468.
19 H. Ishikita, K. Hasegawa and T. Noguchi, *Biochemistry*, 2011, **50**, 5436–5442.
20 T.-J. Lin and P. J. O'Malley, *J. Phys. Chem. B*, 2011, **115**, 4227–4233.
21 R. Chatterjee, S. Milikisiyants, C. S. Coates and K. V. Lakshmi, *Biochemistry*, 2011, **50**, 491–501.
22 Y. Umena, K. Kawakami, J. R. Shen and N. Kamiya, *Nature*, 2011, **473**, 55–60.
23 W. Mäntele, in *Anoxygenic Photosynthetic Bacteria*, ed. R. E. Blankenship, M. T. Madigan and C. E. Bauer, Kluwer Academic Publishers, Dordrecht, The Netherlands, 1995, pp. 627–647.
24 J. Breton and E. Nabedryk, *Biochim. Biophys. Acta*, 1996, **1275**, 84–90.
25 T. Noguchi and C. Berthomieu, in *Photosystem II: The Light-Driven Water:Plastoquinone Oxidoreductase*, ed. T. Wydrzynski and K. Satoh, Springer, Dordrecht, The Netherlands, 2005, pp. 367–387.
26 J. Breton, D. L. Thibodeau, C. Berthomieu, W. Mäntele, A. Vermeglio and E. Nabedryk, *FEBS Lett.*, 1991, **278**, 257–260.
27 J. Breton, C. Boullais, J. R. Burie, E. Nabedryk and C. Mioskowski, *Biochemistry*, 1994, **33**, 14378–14386.
28 R. Brudler, H. J. M. De Groot, W. B. S. Van Liemt, W. F. Steggerda, R. Esmeijer, P. Gast, A. J. Hoff, J. Lugtenburg and K. Gerwert, *EMBO J.*, 1994, **13**, 5523–5530.
29 J. Breton, C. Boullais, G. Berger, C. Mioskowski and E. Nabedryk, *Biochemistry*, 1995, **34**, 11606–11616.
30 E. Nabedryk and J. Breton, *Biochim. Biophys. Acta*, 2008, **1777**, 1229–1248.
31 C. Berthomieu, E. Nabedryk, W. Mäntele and J. Breton, *FEBS Lett.*, 1990, **269**, 363–367.
32 H. Suzuki, M. Nagasaka, M. Sugiura and T. Noguchi, *Biochemistry*, 2005, **44**, 11323–11328.
33 G. Hastings and V. Sivakumar, *Biochemistry*, 2001, **40**, 3681–3689.
34 G. Hastings, K. M. P. Bandaranayake and E. Carrion, *Biophys. J.*, 2008, **94**, 4383–4392.
35 M. Bauscher, E. Nabedryk, K. Bagley, J. Breton and W. Mäntele, *FEBS Lett.*, 1990, **261**, 191–195.
36 M. Bauscher and W. Mäntele, *J. Phys. Chem.*, 1992, **96**, 11101–11108.
37 P. J. O'Malley, *Chem. Phys. Lett.*, 1997, **274**, 251–254.
38 K. S. Raymond, A. K. Grafton and R. A. Wheeler, *J. Phys. Chem. B*, 1997, **101**, 623–631.
39 L. A. Eriksson, F. Himo, P. E. M. Siegbahn and G. T. Babcock, *J. Phys. Chem. A*, 1997, **101**, 9496–9504.
40 N. Mehta and S. N. Datta, *THEOCHEM*, 2008, **870**, 15–22.
41 P. Li, W. H. Wang, H. T. Sun and S. W. Bi, *Comput. Theor. Chem.*, 2013, **1006**, 127–132.
42 D. M. Chipman and M. F. Prebenda, *J. Phys. Chem.*, 1986, **90**, 5557–5560.
43 K. E. Wise, A. K. Grafton and R. A. Wheeler, *J. Phys. Chem. A*, 1997, **101**, 1160–1165.
44 C. G. Zhan and D. M. Chipman, *J. Phys. Chem. A*, 1998, **102**, 1230–1235.
45 M. Nonella, C. Boullais, C. Mioskowski, E. Nabedryk and J. Breton, *J. Phys. Chem. B*, 1999, **103**, 6363–6370.
46 M. R. Razeghifard, S. Kim, J. S. Patzlaff, R. S. Hutchison, T. Krick, I. Ayala, J. J. Steenhuis, S. E. Boesch, R. A. Wheeler and B. A. Barry, *J. Phys. Chem. B*, 1999, **103**, 9790–9800.
47 K. M. P. Bandaranayake, R. L. Wang and G. Hastings, *Biochemistry*, 2006, **45**, 4121–4127.
48 K. M. P. Bandaranayake, R. L. Wang, T. W. Johnson and G. Hastings, *Biochemistry*, 2006, **45**, 12733–12740.
49 M. Nonella, G. Mathias, M. Eichinger and P. Tavan, *J. Phys. Chem. B*, 2003, **107**, 316–322.
50 H. P. Lamichhane and G. Hastings, *Proc. Natl. Acad. Sci. U. S. A.*, 2011, **108**, 10526–10531.
51 E. Martin, A. Baldansuren, T. J. Lin, R. I. Samoilova, C. A. Wraight, S. A. Dikanov and P. J. O'Malley, *Biochemistry*, 2012, **51**, 9086–9093.
52 M. J. Frisch, G. W. Trucks, H. B. Schlegel, G. E. Scuseria, M. A. Robb, J. R. Cheeseman, G. Scalmani, V. Barone, B. Mennucci, G. A. Petersson, H. Nakatsuji, M. Caricato, X. Li, H. P. Hratchian, A. F. Izmaylov, J. Bloino, G. Zheng, J. L. Sonnenberg, M. Hada, M. Ehara, K. Toyota, R. Fukuda, J. Hasegawa, M. Ishida, T. Nakajima, Y. Honda, O. Kitao, H. Nakai, T. Vreven, J. A. Montgomery Jr., J. E. Peralta, F. Ogliaro, M. Bearpark, J. J. Heyd, E. Brothers, K. N. Kudin, V. N. Staroverov, R. Kobayashi, J. Normand, K. Raghavachari, A. Rendell, J. C. Burant, S. S. Iyengar, J. Tomasi, M. Cossi, N. Rega, J. M. Millam, M. Klene, J. E. Knox, J. B. Cross, V. Bakken, C. Adamo, J. Jaramillo, R. Gomperts, R. E. Stratmann, O. Yazyev, A. J. Austin, R. Cammi, C. Pomelli, J. W. Ochterski, R. L. Martin, K. Morokuma, V. G. Zakrzewski, G. A. Voth, P. Salvador, J. J. Dannenberg, S. Dapprich, A. D. Daniels, O. Farkas, J. B. Foresman,

J. V. Ortiz, J. Cioslowski and D. J. Fox, *Gaussian 09, Revision C.01*, Gaussian, Inc., Wallingford, CT, 2009.
53 A. D. Becke, *J. Chem. Phys.*, 1993, **98**, 5648–5652.
54 C. Lee, W. Yang and R. G. Parr, *Phys. Rev. B: Condens. Matter Mater. Phys.*, 1988, **37**, 785–789.
55 E. Cances, B. Mennucci and J. Tomasi, *J. Chem. Phys.*, 1997, **107**, 3032–3041.
56 B. Mennucci and J. Tomasi, *J. Chem. Phys.*, 1997, **106**, 5151–5158.
57 B. Mennucci, E. Cances and J. Tomasi, *J. Phys. Chem. B*, 1997, **101**, 10506–10517.
58 S. Trasatti, *Pure Appl. Chem.*, 1986, **58**, 955–966.
59 H. Reiss and A. Heller, *J. Phys. Chem.*, 1985, **89**, 4207–4213.
60 R. C. Prince, P. L. Dutton and J. M. Bruce, *FEBS Lett.*, 1983, **160**, 273–276.
61 M. K. Gilson and B. H. Honig, *Biopolymers*, 1986, **25**, 2097–2119.
62 H. Nakamura, T. Sakamoto and A. Wada, *Protein Eng.*, 1988, **2**, 177–183.
63 C. D. Cooper, W. T. Naff and R. N. Compton, *J. Phys. Chem.*, 1975, **63**, 2752–2757.
64 S. Chowdhury, T. Heinis, E. P. Grimsrud and P. Kebarle, *J. Phys. Chem.*, 1986, **90**, 2747–2752.
65 T. Heinis, S. Chowdhury, S. L. Scott and P. Kebarle, *J. Am. Chem. Soc.*, 1988, **110**, 400–407.
66 A. M. Weyers, R. Chatterjee, S. Milikisiyants and K. V. Lakshmi, *J. Phys. Chem. B*, 2009, **113**, 15409–15418.
67 K. Hasegawa and T. Noguchi, *Biochemistry*, 2005, **44**, 8865–8872.
68 J. S. Jaworski, E. Lesniewska and M. K. Kalinowski, *J. Electroanal. Chem.*, 1979, **105**, 329–334.
69 X. J. Zhao and T. Kitagawa, *J. Raman Spectrosc.*, 1998, **29**, 773–780.
70 M. E. Peover, *J. Chem. Soc.*, 1962, 4540–4549.
71 N. Gupta and H. Linschitz, *J. Am. Chem. Soc.*, 1997, **119**, 6384–6391.
72 K. S. Feldman, D. K. Hester II and J. H. Golbeck, *Bioorg. Med. Chem. Lett.*, 2007, **17**, 4891–4894.
73 C. S. Coates, J. Ziegler, K. Manz, J. Good, B. Kang, S. Milikisiyants, R. Chatterjee, S. J. Hao, J. H. Golbeck and K. V. Lakshmi, *J. Phys. Chem. B*, 2013, **117**, 7210–7220.
74 J. Kruk, K. Strzalka and R. M. Leblanc, *Biophys. Chem.*, 1993, **45**, 235–244.
75 J.-R. Burie, A. Boussac, C. Boullais, G. Berger, T. Mattioli, C. Mioskowski, E. Nabedryk and J. Breton, *J. Phys. Chem.*, 1995, **99**, 4059–4070.
76 R. A. Wheeler, *J. Phys. Chem.*, 1993, **97**, 1533–1537.
77 T. Noguchi, T. Ono and Y. Inoue, *Biochim. Biophys. Acta*, 1995, **1228**, 189–200.
78 R. Takahashi, K. Hasegawa, A. Takano and T. Noguchi, *Biochemistry*, 2010, **49**, 5445–5454.

